Supporting Information: On Reaction Pathways and Intermediates During Catalytic Olefin Cracking over ZSM-5

Sebastian Standl,[†,‡] Tobias Kühlewind,[†,‡] Markus Tonigold,[¶] and Olaf Hinrichsen[*,†,‡]

†Department of Chemistry, Technical University of Munich, Lichtenbergstraße 4, 85748 Garching Near Munich, Germany

‡Catalysis Research Center, Technical University of Munich, Ernst-Otto-Fischer-Straße 1, 85748 Garching Near Munich, Germany

¶Clariant Produkte (Deutschland) GmbH, Waldheimer Straße 13, 83052 Bruckmühl, Germany

E-mail: olaf.hinrichsen@ch.tum.de

Phone: +49 (89) 289 13232. Fax: +49 (89) 289 13513

1 Cracking Reactivity

In the original reaction network,[1] the following rules were applied to the molecular structure of olefins:

- maximum carbon number of twelve,

- exclusion of quaternary carbon atoms,

- only methyl side groups,

- maximum number of methyl side groups of two per compound,

- exclusion of all 2,3-dimethylbutenes,

- exclusion of further sterically demanding compounds.

These assumptions result from experimental observations.[2–5] All included species can participate in different types of elementary reactions, again according to several rules,[1] which are shown in Scheme S1.
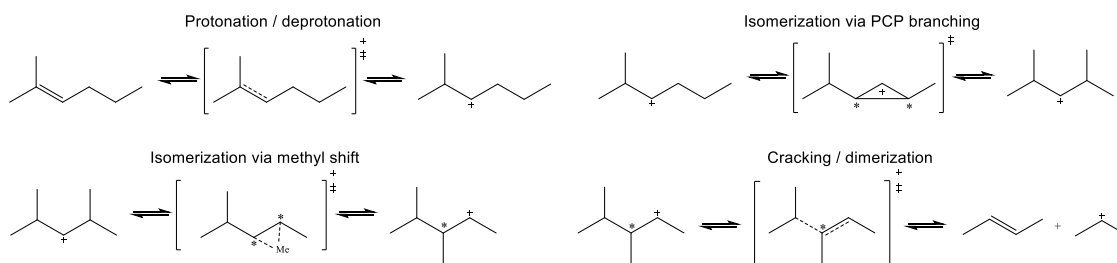

Scheme S1: Different types of elementary reactions that are included in the single-event kinetic model.

Protonation of the double bond of an olefin leads to a protonated intermediate whereas the backward reaction, the deprotonation, releases the corresponding olefin. The protonated intermediate can undergo isomerization reactions: through a methyl shift, the positive charge and the methyl side group switch position. In another type of methylation reaction, a protonated cyclopropane evolves as transition state. Then, one of the three bonds breaks and leads

to the product. Because of the elevated temperatures during cracking, both (de)protonation and isomerization reactions are assumed as *quasi*-equilibrated.[6] In contrast, cracking of a protonated intermediate is a step of kinetic relevance. The same holds for the backward reaction, the dimerization, where a smaller protonated intermediate and an olefin react to a larger protonated intermediate.

2 Reaction Network

An overview of the different reaction networks analyzed in the preliminary study can be found in Scheme S2.
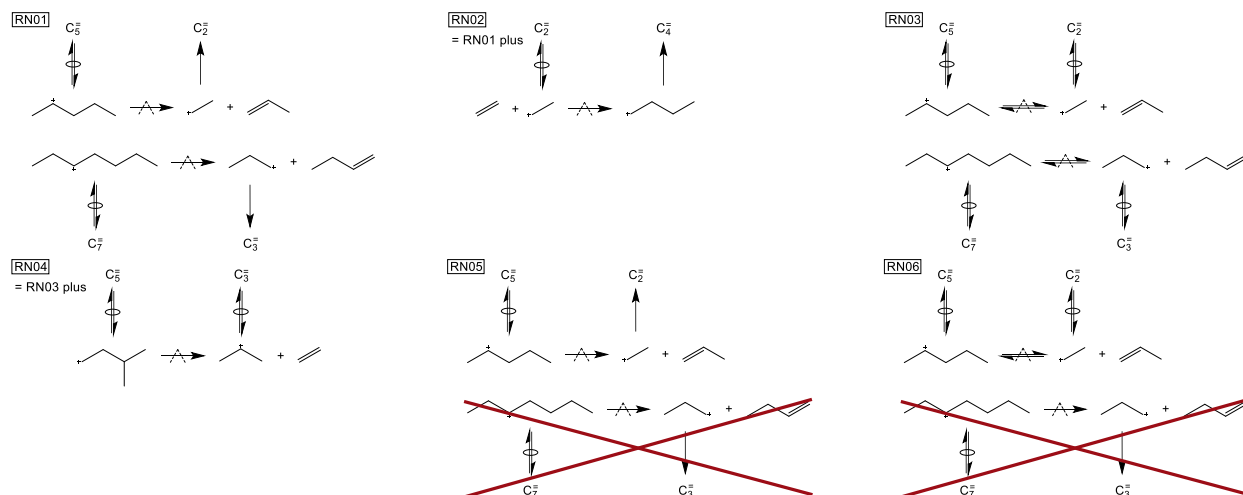
Scheme S2: Differences between all six reaction networks analyzed in a preliminary study with respect to the role of primary intermediates.

RN01 is the original one[1] where primary intermediates of all carbon lengths between C_2 and C_{10} are formed. RN02 includes the self-dimerization of ethene to C_4 which causes one additional protonation (ethene to ethyl) and one additional dimerization reaction. In RN03, the protonation to the primary intermediates of each carbon number is required and therefore allowed since the cracking to primary intermediates is assumed to be reversible here. A further extension is made in RN04: Because the protonation to primary intermediates is allowed according to RN03, the subsequent cracking of these intermediates might occur and

is thus considered. In contrast to that, the original network is reduced in RN05: cracking to primary intermediates is only possible when ethene is formed. Finally, in RN06, the steps leading to ethene are assumed to be reversible. Table S1 is similar to Table 1 in the main text, but additionally contains the values for RN02–05.

Table S1: Type of elementary reactions being implemented in the single-event kinetic model for olefin cracking, including the amount of different reactions and of kinetically relevant steps for all six reaction networks; furthermore, the number of different olefins and protonated intermediates is shown.

type	RN01	RN02	RN03	RN04	RN05	RN06
olefin protonation	956	957	1095	1095	956	957
cracking	601	601	601	636	238	238
pathways cracking	1292	1292	1292	1327	511	511
dimerization	140	141	601	601	140	238
pathways dimerization	293	294	1292	1292	293	511
PCP branching	1530	1530	1530	1530	1530	1530
methyl shift	148	148	148	148	148	148
olefin deprotonation	1004	1004	1095	1095	957	957
olefins	591	591	591	591	591	591
protonated intermediates	498	498	589	589	451	451

An application of the six different reaction networks to the kinetic model leads to the results in Table S2, which again is similar to its counterpart in the main text, Table 2, but extended with the results of RN02–05.

Table S2: Estimated activation energies E_a^{cr} and pre-exponential factors A^{cr}, including 95% confidence intervals, and the sum of squared residuals SSQ for all six reaction networks; all activation energies are given in $kJ\,mol^{-1}$, whereas the pre-exponential factor is shown in s^{-1}.

parameter	RN01	RN02	RN03	RN04	RN05	RN06
$E_a^{cr}(s;p)$	229.9 ± 1.0	229.3 ± 1.1	229.4 ± 1.0	233.1 ± 51.7	229.9 ± 1.0	229.6 ± 1.0
$E_a^{cr}(s;s)$	200.2 ± 0.9	199.9 ± 1.0	199.7 ± 0.9	199.5 ± 1.0	200.1 ± 0.9	199.8 ± 0.9
$E_a^{cr}(t;s)$	171.5 ± 0.9	171.1 ± 1.0	171.0 ± 0.9	170.9 ± 1.1	171.5 ± 0.9	171.2 ± 0.9
$E_a^{cr}(t;p)$	211.9 ± 1.5	211.4 ± 1.6	210.5 ± 1.6	210.5 ± 4.4	212.0 ± 1.6	210.7 ± 1.5
$\widetilde{A}^{cr} \times 10^{-16}$	2.73 ± 0.40	2.53 ± 0.41	2.51 ± 0.36	2.45 ± 0.47	2.73 ± 0.41	2.59 ± 0.38
SSQ	0.0350	0.0348	0.0345	0.0341	0.0350	0.0345

RN02 shows a slightly better description of the experiments and thus a lower SSQ value, which can be explained by the use of an additional parameter to describe the self-dimerization

of ethene. The estimated value of $E_a^{cr}(p;p)$ is $206.0 \pm 5.7\,\text{kJ}\,\text{mol}^{-1}$. The almost insignificant improvement means this pathway is irrelevant at cracking conditions due to high temperatures and comparably low ethene fractions. However, the fact that this parameter can be estimated to a reasonable and significant value without changing the results of the other activation energies suggests this pathway to be present. Furthermore, the improvement in describing the experimental data is mainly caused by ethene, which also speaks for the general occurrence of this step. Consequently, the neglection of ethene self-dimerization is an assumption suitable for typical cracking conditions, but care should be taken when extrapolating the model to conditions in which this hypothesis might not be true; in such cases, the parameter $E_a^{cr}(p;p)$ should be included.

An improvement in agreement is found for RN03 where all steps leading to primary intermediates are reversible, increasing the number of (de)protonation and dimerization reactions and therefore the numerical effort to a significant extent.

When the protonation to primary intermediates is allowed, their subsequent cracking might also take place, especially when it offers a transformation to a product intermediate of higher stability. This is why the additional parameter $E_a^{cr}(p;s)$ is introduced for RN04; it can be estimated to a value of $233.3 \pm 56.5\,\text{kJ}\,\text{mol}^{-1}$. The high confidence interval, which is also obtained for the cracking step (s;p) in RN04, shows numeric problems when applying this reaction network. For that reason, the underlying pathways are questionable, although the description is the best one found in Table S2.

The analysis of RN05 shows that an agreement of equal quality compared to RN01 is obtained although cracking to primary product intermediates is only allowed when this step produces ethene. This leads to less cracking and deprotonation reactions and thus to a faster fitting process. It can be stated that except for ethene formation, the cracking to primary intermediates is irrelevant for energetic reasons and should be therefore left out.

Finally, an improved agreement is found for RN06 in which the ethene formation steps from RN05 are assumed to be reversible. The quality of description is similar to RN03, which

underlines that in both models, the improvement can be fully ascribed to the reversible ethene formation steps.

3 Mathematical Description of Adsorption

Nguyen et al.[7] provide parameters α to δ for the evolution of a π-complex as well as for the chemisorption of linear olefins on ZSM-5 (Si/Al of 95). The authors investigated chain lengths between C_2 and C_8 (1-alkenes), between C_4 and C_8 (2-alkenes) as well as C_6 and C_8 (3-alkenes) and 4-octene. Two different parameter sets are shown, one for 1-alkenes and another one for 2-/3-/4-alkenes. In addition, a separate fit of the chemisorption enthalpy of 1-alkenes with chain lengths between C_2 and C_5 is given. The values resulted from a theoretical DFT study that combined quantum mechanics and molecular mechanics. This QM-Pot technique originally developed by Sauer and coworkers[8–11] was combined with statistical thermodynamic calculations. Besides the interaction between the double bond and the acid site, these values contain van der Waals contributions resulting from the corrected Lennard-Jones potentials derived earlier.[12] In the regular Nguyen correlations,[7] chemisorption leads to secondary alkoxides. In a conference paper authored by the same group,[13] a correlation is given that allows for the description of the formation of a tertiary alkoxide. However, a linear coherence was only obtained for the sum of the chemisorption enthalpy and the standard enthalpy of formation.[13] A similar fit was performed for the chemisorption to secondary alkoxides out of 1-alkenes or 2-/3-/4-alkenes, respectively. Finally, the special case of isobutene adsorption was treated in a separate publication,[14] including formation of π-complex, alkoxide and carbenium ion.

For alkanes, two different main concepts to measure physisorption effects exist in literature. Lercher and coworkers[15,16] determined the physisorption enthalpy using calorimetry, whereas the Langmuir coefficient was fitted to experimental data. From these values, the thermodynamic equilibrium constant is accessible and the physisorption entropy is obtained

using Eq. S1,

$$\Delta_{\text{phys}} S_i^\circ = R \ln \left(K^{\text{phys}} (i) \right) + \frac{\Delta_{\text{phys}} H_i^\circ}{T}. \tag{S1}$$

The similar methodology lead to the experimental results of de Moor et al.[12] In this study, other physisorption values from literature are additionally listed and compared. Furthermore, the authors provide both experimental and theoretical physisorption parameters α to δ. In the following, experimentally derived values are used that were obtained with a ZSM-5 catalyst (Si/Al of 35), with n-alkanes between C_3 and C_6 as feed and at temperatures between 301 and 400 K.

In contrast, Denayer et al.[17,18] applied a pulse chromatographic technique which is only valid in the linear Henry regime, i.e., when pressures are low. This methodology yielded the Henry constant according to Eq. S2:

$$K^{\text{H}} (i) = K_0^{\text{H}} (i) \, \exp \left(-\frac{\Delta_{\text{phys}} H_i^\circ}{RT} \right). \tag{S2}$$

The physisorption enthalpy was derived from the temperature dependence of $K^{\text{H}} (i)$. In addition, the physisorption entropy was related to the pre-exponential Henry factor $K_0^{\text{H}} (i)$, see Eq. S3,

$$\Delta_{\text{phys}} S_i^\circ = R \ln \left(\frac{2 \, p^\circ \, K_0^{\text{H}} (i)}{C_{\text{t}}} \right). \tag{S3}$$

Physisorption parameters α to δ are provided by the authors to calculate enthalpy and the natural logarithm of $K_0^{\text{H}} (i)$. Two data sets are given, accounting for linear and 2-methyl branched alkanes. These were derived from experiments with ZSM-5 (Si/Al of 137) at temperatures between 548 and 648 K using linear and branched C_5 to C_8 alkanes as feed.

Both methodologies can be compared in the low-pressure region which is shown in Eq. S4,

$$K^{\text{H}} (i) = C^{\text{sat}} (i) \, K_{\text{L}}^{\text{phys}} (i). \tag{S4}$$

Both sides are converted so that the thermodynamic equilibrium constant is obtained, see

Eq. S5,

$$\frac{C_{\text{t}}}{2\,p^{\circ}} K^{\text{phys}}(i) = \frac{C^{\text{sat}}(i)}{p^{\circ}} K^{\text{phys}}(i).$$ (S5)

Whereas the approach by Lercher and co-workers[15,16] accounts for hydrocarbon-specific saturation effects on the catalytic surface, the carbon number independent value of the acid sites' concentration is used for Denayer et al.[17,18] The deviation is significant especially for ZSM-5, leading in the latter case to physisorption entropies which are increased about $25\,\text{J}\,\text{mol}^{-1}\,\text{K}^{-1}$. Because of this, revised entropy values for Denayer are given by de Moor et al.[12] stemming from an application of Eq. S6,

$$\Delta_{\text{phys}}S_i^{\circ} = R\,\ln\left(\frac{p^{\circ}\,K_{0,i}^{\text{H}}}{C^{\text{sat}}(i)}\right).$$ (S6)

4 Additional material for Section 3.3.1
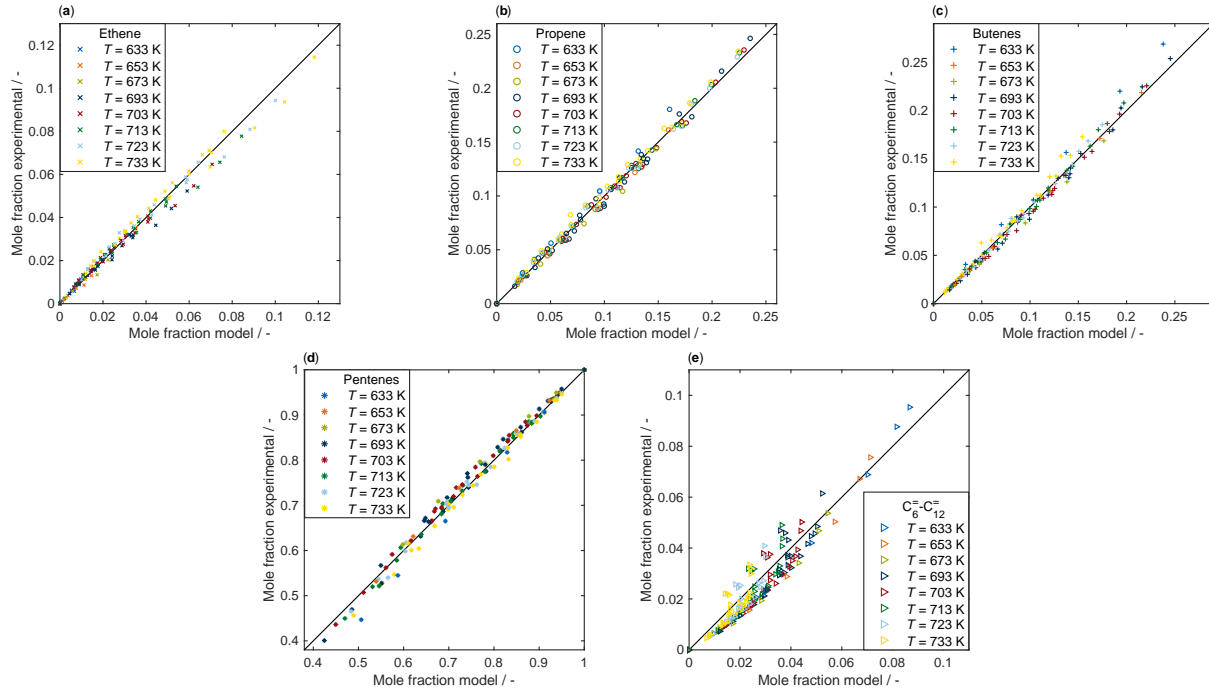
Figure S1: Parity plots for ethene, (a), propene, (b), butenes, (c), pentenes, (d), and C_6 to C_{12} olefins, (e), resulting from an application of model no. 01, see Table 3.
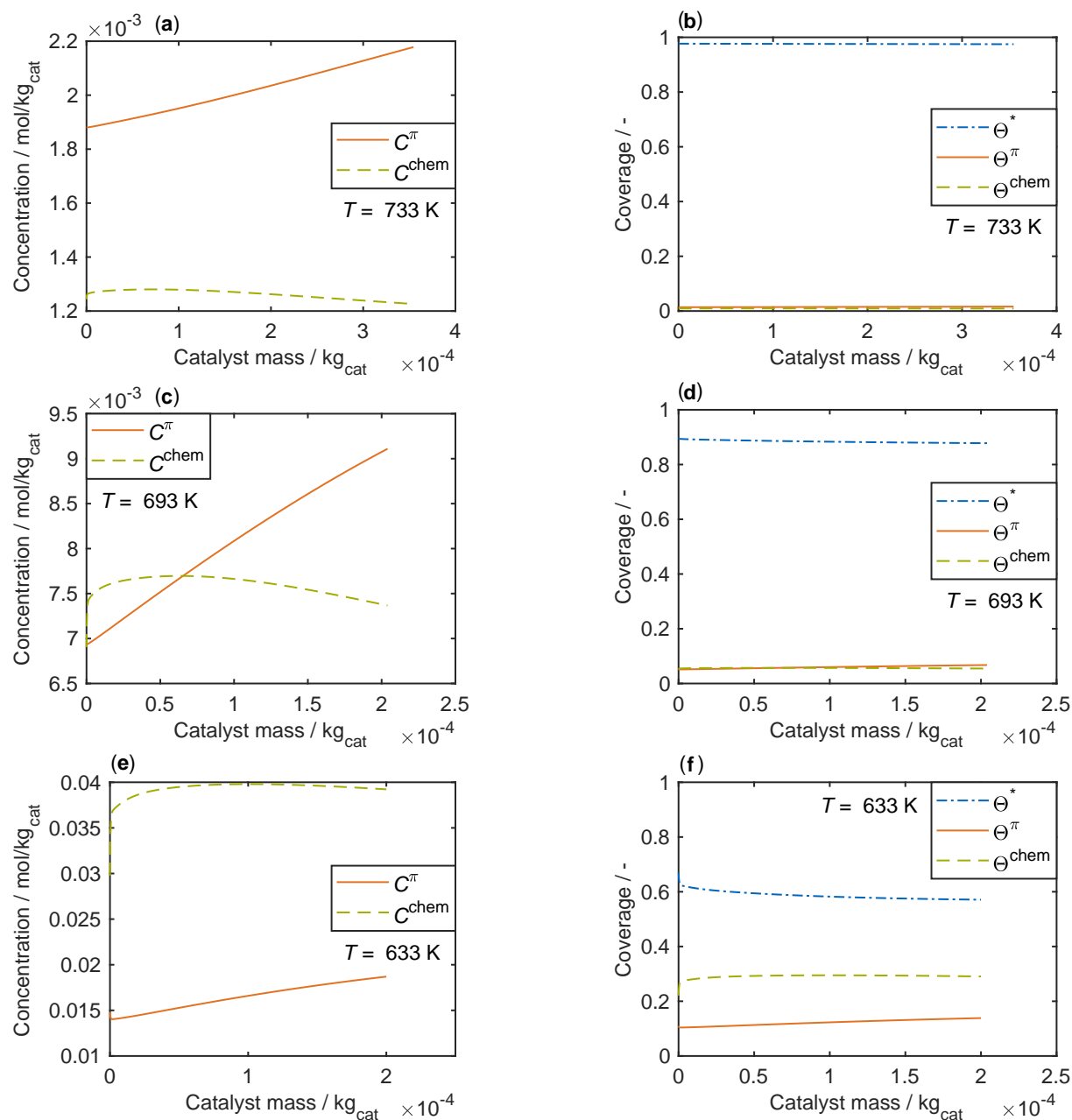
Figure S2: Total concentration of adsorbed species, either π-complex or chemisorption, (a), (c) and (e), and relative coverages or amount of free acid sites, (b), (d) and (f), at three different reaction conditions: $733\,\mathrm{K}$ and inlet partial pressure of 1-pentene $p_{\mathrm{C5}}^{\mathrm{in}} = 42.7\,\mathrm{mbar}$, (a) and (b), $693\,\mathrm{K}$ and $p_{\mathrm{C5}}^{\mathrm{in}} = 70.3\,\mathrm{mbar}$, (c) and (d), $633\,\mathrm{K}$ and $p_{\mathrm{C5}}^{\mathrm{in}} = 42.7\,\mathrm{mbar}$, (e) and (f); the total pressure p_{t} is set to $1.23\,\mathrm{bar}$ for all subfigures.
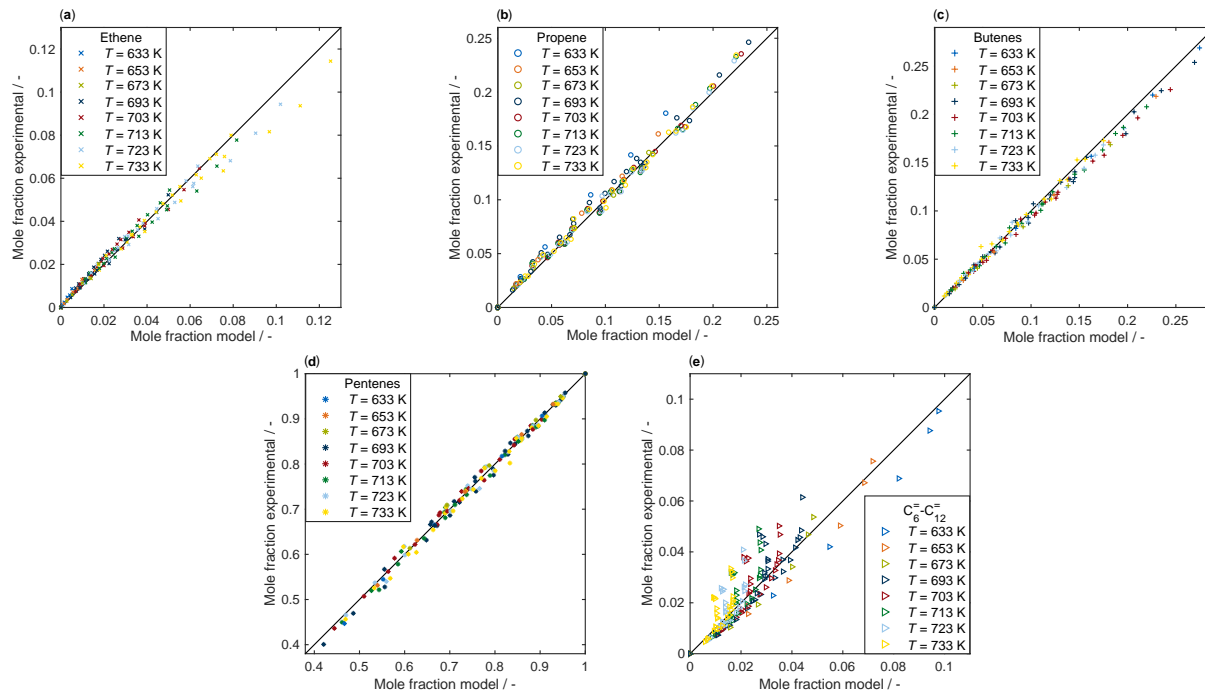
Figure S3: Parity plots for ethene, (a), propene, (b), butenes, (c), pentenes, (d), and C_6 to C_{12} olefins, (e), resulting from an application of model no. 02, see Table 3.
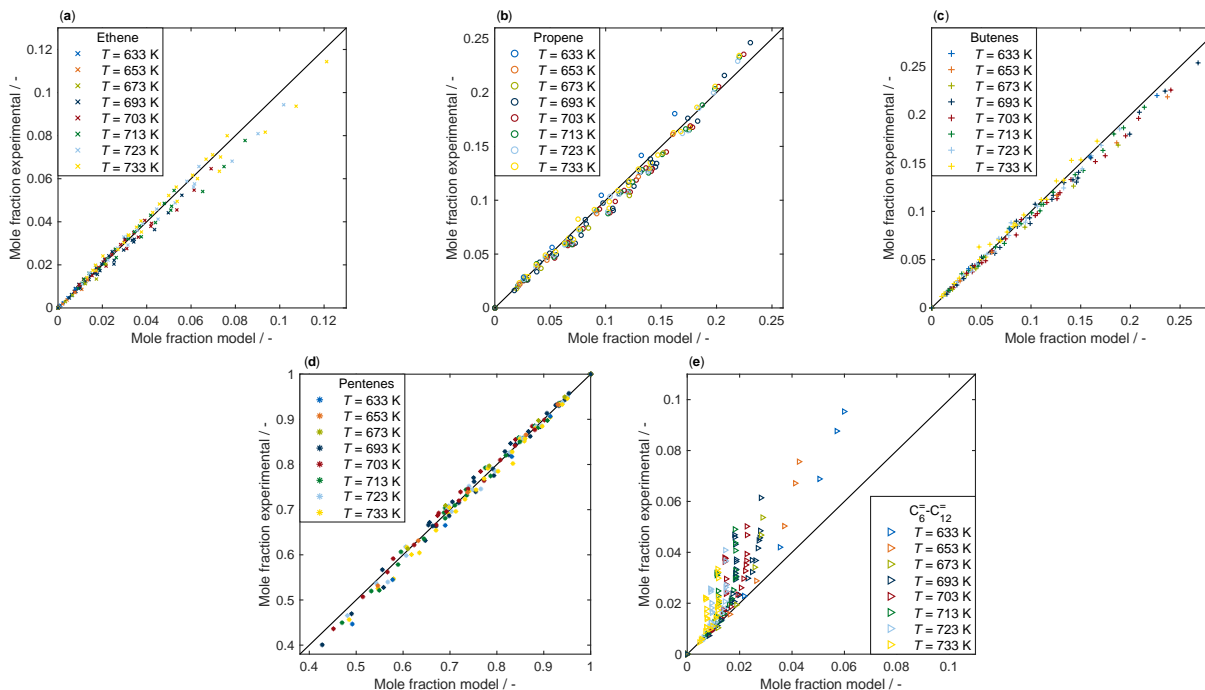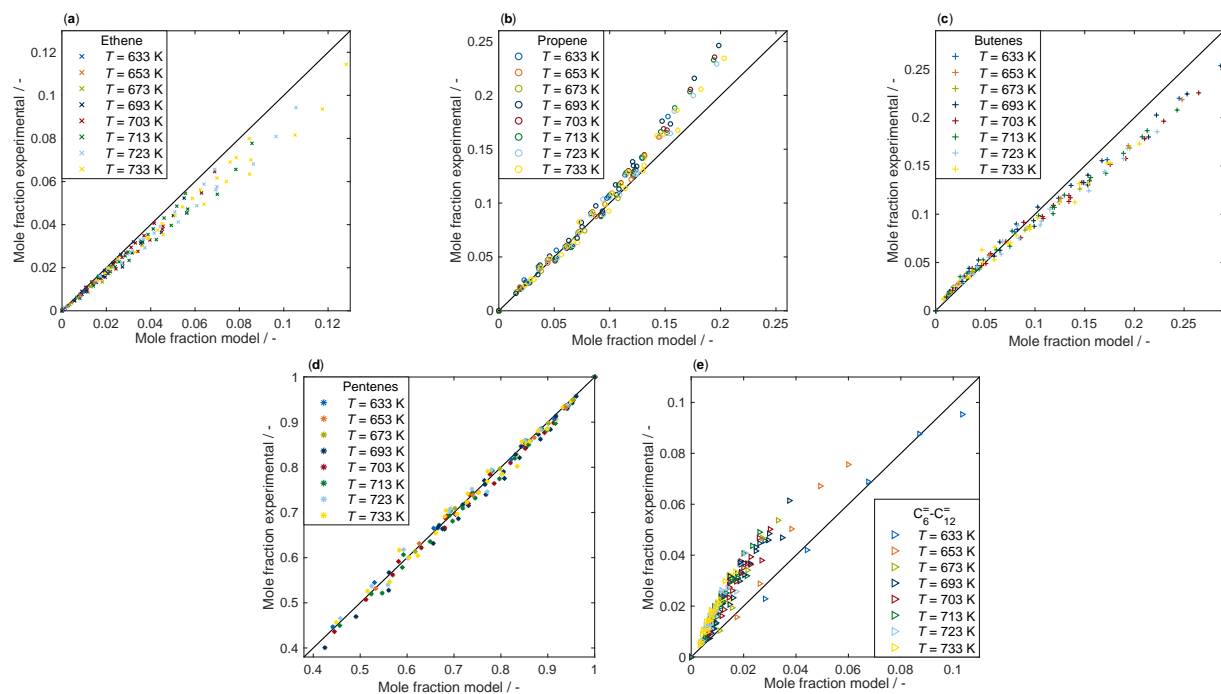

Figure S4: Parity plots for ethene, (a), propene, (b), butenes, (c), pentenes, (d), and C_6 to C_{12} olefins, (e), resulting from an application of model no. 03, see Table 3.

5   Additional material for Section 3.3.2

Figure S5: Parity plots for ethene, (a), propene, (b), butenes, (c), pentenes, (d), and C_6 to C_{12} olefins, (e), resulting from an application of model no. 04, see Table 4.
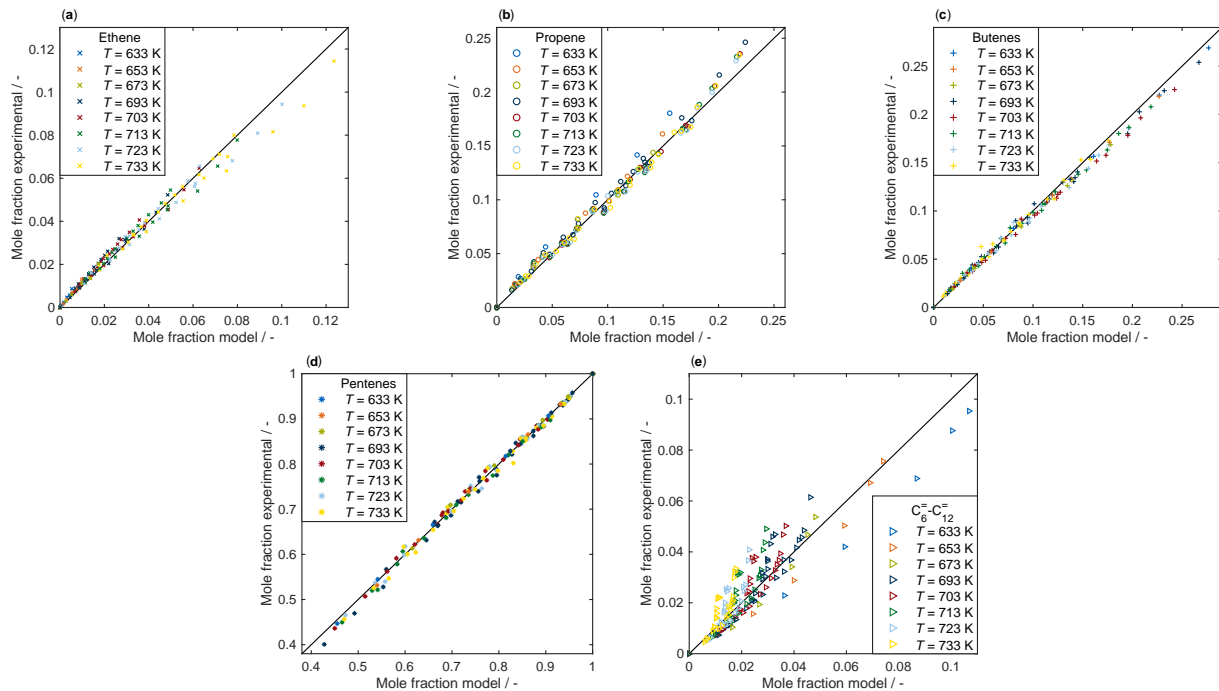
Figure S6: Parity plots for ethene, (a), propene, (b), butenes, (c), pentenes, (d), and C_6 to C_{12} olefins, (e), resulting from an application of model no. 05, see Table 4.
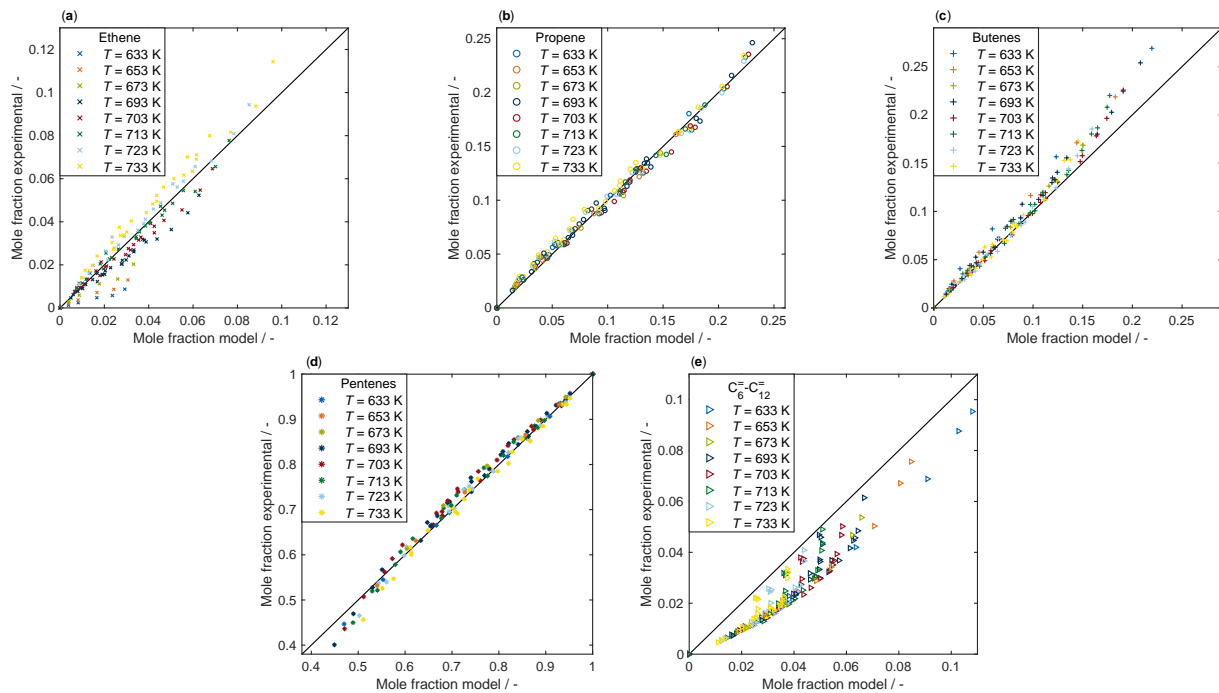

Figure S7: Parity plots for ethene, (a), propene, (b), butenes, (c), pentenes, (d), and C_6 to C_{12} olefins, (e), resulting from an application of model no. 06, see Table 4.
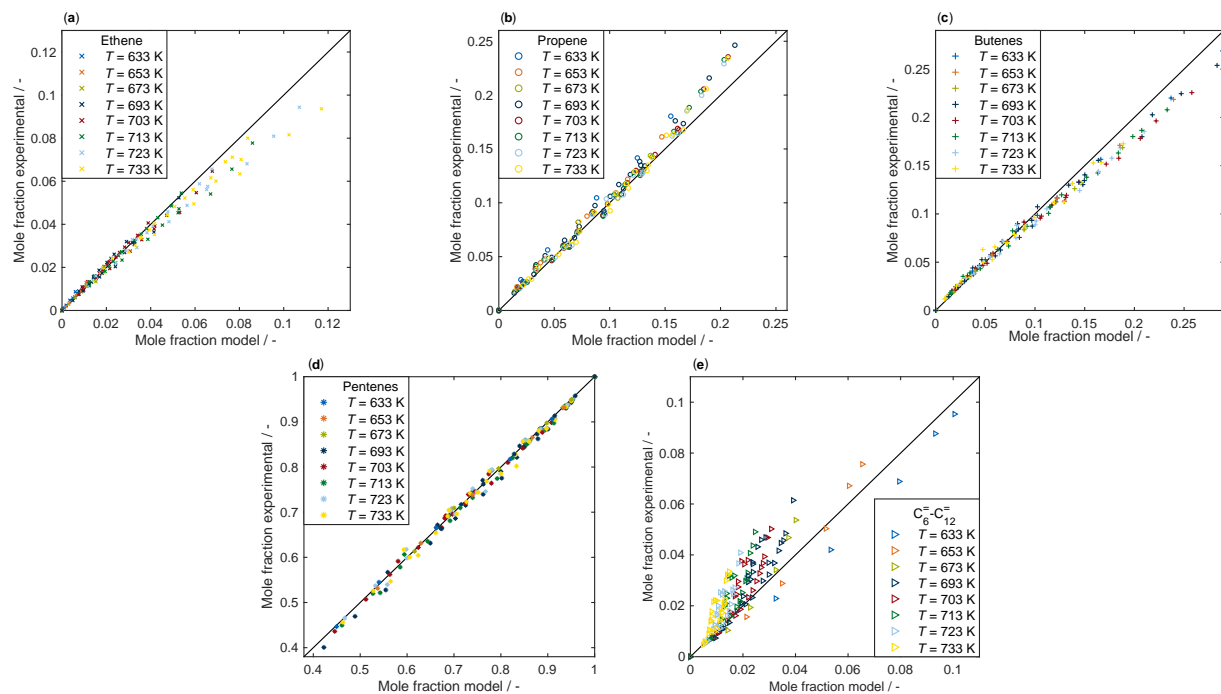
Figure S8: Parity plots for ethene, (a), propene, (b), butenes, (c), pentenes, (d), and C_6 to C_{12} olefins, (e), resulting from an application of model no. 07, see Table 4.

References

(1) von Aretin, T.; Schallmoser, S.; Standl, S.; Tonigold, M.; Lercher, J. A.; Hinrichsen, O. Single-Event Kinetic Model for 1-Pentene Cracking on ZSM-5. *Ind. Eng. Chem. Res.* **2015**, *54*, 11792–11803.

(2) Garwood, W. E. In *Intrazeolite Chemistry*; Stucky, G. D., Dwyer, F. G., Eds.; ACS Symposium Series; American Chemical Society: Washington, D.C., USA, 1983; Vol. 218; pp 383–396.

(3) Abbot, J.; Wojciechowski, B. W. Catalytic Cracking and Skeletal Isomerization of *n*-Hexene on ZSM-5 Zeolite. *Can. J. Chem. Eng.* **1985**, *63*, 451–461.

(4) Abbot, J.; Wojciechowski, B. W. The Mechanism of Catalytic Cracking of *n*-Alkenes on ZSM-5 Zeolite. *Can. J. Chem. Eng.* **1985**, *63*, 462–469.

(5) Tabak, S. A.; Krambeck, F. J.; Garwood, W. E. Conversion of Propylene and Butylene over ZSM-5 Catalyst. *AIChE J.* **1986**, *32*, 1526–1531.

(6) Thybaut, J. W.; Marin, G. B.; Baron, G. V.; Jacobs, P. A.; Martens, J. A. Alkene Protonation Enthalpy Determination from Fundamental Kinetic Modeling of Alkane Hydroconversion on Pt/H-(US)Y-Zeolite. *J. Catal.* **2001**, *202*, 324–339.

(7) Nguyen, C. M.; de Moor, B. A.; Reyniers, M.-F.; Marin, G. B. Physisorption and Chemisorption of Linear Alkenes in Zeolites: A Combined QM-Pot(MP2//B3LYP:GULP)-Statistical Thermodynamics Study. *J. Phys. Chem. C* **2011**, *115*, 23831–23847.

(8) Sauer, J.; Sierka, M. Combining Quantum Mechanics and Interatomic Potential Functions in Ab Initio Studies of Extended Systems. *J. Comput. Chem.* **2000**, *21*, 1470–1493.

(9) Sierka, M.; Sauer, J. Proton Mobility in Chabazite, Faujasite, and ZSM-5 Zeolite Cat-

alysts. Comparison Based on ab Initio Calculations. *J. Phys. Chem. B* **2001**, *105*, 1603–1613.

(10) Clark, L. A.; Sierka, M.; Sauer, J. In *Impact of Zeolites and other Porous Materials on the new Technologies at the Beginning of the New Millennium*; Aiello, R., Giordano, G., Testa, F., Eds.; Studies in Surface Science and Catalysis; Elsevier: Amsterdam, NLD, 2002; Vol. 142; pp 643–649.

(11) Nachtigall, P.; Sauer, J. In *Introduction to Zeolite Science and Practice*; Čejka, J., van Bekkum, H., Corma, A., Schüth, F., Eds.; Studies in Surface Science and Catalysis; Elsevier: Amsterdam, NLD, 2007; Vol. 168; pp 701–738.

(12) de Moor, B. A.; Reyniers, M.-F.; Gobin, O. C.; Lercher, J. A.; Marin, G. B. Adsorption of C2-C8 *n*-Alkanes in Zeolites. *J. Phys. Chem. C* **2011**, *115*, 1204–1219.

(13) Nguyen, C. M.; de Moor, B. A.; Reyniers, M.-F.; Marin, G. B. Effect of Nanopore Dimension and Network Topology on Alkene Sorption Thermodynamics. 2nd International Workshop NAPEN, Rhodes, Greece, June 09–11. 2011.

(14) Nguyen, C. M.; de Moor, B. A.; Reyniers, M.-F.; Marin, G. B. Isobutene Protonation in H-FAU, H-MOR, H-ZSM-5, and H-ZSM-22. *J. Phys. Chem. C* **2012**, *116*, 18236–18249.

(15) Eder, F.; Lercher, J. A. Alkane Sorption in Molecular Sieves: The Contribution of Ordering, Intermolecular Interactions, and Sorption on Brønsted Acid Sites. *Zeolites* **1997**, *18*, 75–81.

(16) Eder, F.; Stockenhuber, M.; Lercher, J. A. Brønsted Acid Site and Pore Controlled Siting of Alkane Sorption in Acidic Molecular Sieves. *J. Phys. Chem. B* **1997**, *101*, 5414–5419.

(17) Denayer, J. F.; Baron, G. V.; Martens, J. A.; Jacobs, P. A. Chromatographic Study of

Adsorption of *n*-Alkanes on Zeolites at High Temperatures. *J. Phys. Chem. B* **1998**, *102*, 3077–3081.

(18) Denayer, J. F.; Souverijns, W.; Jacobs, P. A.; Martens, J. A.; Baron, G. V. High-Temperature Low-Pressure Adsorption of Branched C_5–C_8 Alkanes on Zeolite Beta, ZSM-5, ZSM-22, Zeolite Y, and Mordenite. *J. Phys. Chem. B* **1998**, *102*, 4588–4597.